PNAS
www.pnas.org

Main Manuscript for

Mechanisms of lipid preservation in archaeological clay ceramics revealed by mass spectrometry imaging

Simon Hammann[1,2 *], David J. Scurr[3], Morgan R. Alexander[3], Lucy J. E. Cramp[1]

[1] Department of Anthropology and Archaeology, University of Bristol, 43 Woodland Road, Bristol BS8 1UU, United Kingdom

[2] Department of Chemistry and Pharmacy, Friedrich-Alexander University Erlangen-Nürnberg, Nikolaus-Fiebiger Straße 10, 91058 Erlangen, Germany

[3] Advanced Materials and Healthcare Technologies, School of Pharmacy, University of Nottingham, Nottingham NG7 2TQ, United Kingdom

*corresponding author:

Simon Hammann
Friedrich-Alexander University Erlangen-Nürnberg
Nikolaus-Fiebiger Straße 10
91058 Erlangen, Germany
Email: simon.hammann@fau.de
Phone: +49 9131 8565391

ORCID: Simon Hammann: 0000-0002-4311-7351; David J. Scurr: 0000-0003-0859-3886; Morgan R. Alexander: 0000-0001-5182-493X; Lucy J. E. Cramp: 0000-0003-2012-2753

Classification

Physical Sciences/Chemistry

Social Sciences/Anthropology

Keywords

Lipid, Archaeology, Mass Spectrometry Imaging, SIMS

This PDF file includes:

Main Text
Figures 1 to 3
Table 1

Abstract

Traces of lipids, absorbed and preserved for millennia within the inorganic matrix of ceramic vessels, act as molecular fossils and provide manifold information about past people's subsistence, diet and rituals. It is widely assumed that lipids become preserved after adsorption into nano- to micrometer sized pores, but to this day the distribution of these lipids in the ceramics was virtually unknown, which severely limits our understanding about the process of lipid preservation. Here we use secondary ion mass spectrometry (SIMS) imaging for the first direct *in situ* analysis of lipids absorbed in 700 – 2000 year old archaeological pottery. After sectioning from larger sherds, wall cross sections of smaller fragments were used for SIMS analysis. Lipids were found in relatively large zones of 5 – 400 µm in diameter which does not support the notion of absorption only into individual nanometer-scale pores but indicates that more macroscopic structures in the ceramics are involved in lipid preservation as well. Furthermore, lipids were found concentrated on calcium carbonate inclusions in the ceramics, which suggests that precipitation of fatty acids as calcium salts is an important aspect of lipid preservation in archaeological samples. This has important implications for analytical methods based on extraction of lipids from archaeological ceramics and needs to be considered to maximize the yield and available information from each unique sample.

Significance Statement

Lipids, preserved in archaeological ceramics, offer unique insights into past people's diets and cultural practices. Yet, the fundamental question of how lipids are preserved for millennia is not clear. This study describes the first direct visualisation of lipids in wall cross sections of archaeological potsherds using mass spectrometry imaging. Lipids were distributed unevenly in zones of >200 µm size, indicating that macroscopic structures and properties, and not only small pores, facilitate lipid preservation. We also show the formation of calcium fatty acid salts as an additional aspect of lipid preservation. These findings have important implications for the selection of appropriate methods for lipid analysis in potsherds and show that the analysis of lipid distribution patterns could improve and refine interpretations.

Main Text

Introduction

Fragments of ceramic cooking vessels are frequently encountered in archaeological excavations. In addition to their macroscopic properties (e.g. shape or decoration) these fragments carry unique information about customs, diet and technology of past societies through preserved chemical remnants (1). Lipids (and other constituents) from food items are liberated and absorbed into the porous ceramic matrix during cooking processes in unglazed pots. Traces of these lipids (often < 100 µg/g ceramics) can be preserved in fragments of the pots for several millennia, while undergoing molecular alteration processes that lead to structurally-characteristic transformation products (1, 2). Most commonly, saturated fatty acids and - to a lesser degree - simple acyl lipids (triacylglycerols, wax esters) are detected. The analysis of the molecular identity, as well as stable isotope signature of these preserved lipid residues, using sensitive chromatographic and mass spectrometric techniques is collectively referred to as Organic Residue Analysis (ORA) (1). This has been used in previous studies to great effect to answer fundamental questions about early human history such as the identification of specific food sources, implementation and spread of dairy processing, cereal and plant consumption and the exploitation of honey bee products (3-7).

However, even after several decades of applying ORA and the analysis of thousands of samples, it is still unclear how this preservation of lipids is actually realised. It is widely assumed that small pores in the ceramics (in the order of some nanometers to several micrometers) act as a safe haven for lipids, protecting them from microbial degradation and ground-water leaching (2, 8). Previous studies also suggested that lipids bind and interact with the ceramic surface revealing specific, ceramic-dependent reactions (9-11). However, the hypothesised role of the ceramic matrix in lipid preservation has never been tested directly in microscopic detail and the precise distribution of lipids within the ceramic matrix of archaeological pottery is virtually unknown. As a fundamental principle underpinning ORA it is of high importance to understand the interaction between ceramics and lipids, as this would allow better sampling, analytical strategies and to refine the interpretation of results regarding human past practices and foodways.

The usual protocols for ORA are destructive and require the ceramic samples to be powdered prior to solvent extraction and instrumental analysis. As such, the data are devoid of any spatial information. In 2000, Stern et al. extracted and analysed lipids from 2 mm layers of ceramic sherds and observed a decreasing concentration gradient from the inside (i.e. orientated towards pot contents) to outside surface (12). However, the resolution achieved in using this

approach was macroscopic and unable to provide a detailed view elucidating the role of the ceramic fine structure. Recently, Goldenberg et al. attempted to determine the distribution of lipids by a combination of iodine addition to lipid double bonds and subsequent X-ray mapping (13) but the method was limited by its indirect and unspecific nature, the absence of molecular information as well as cross-reactions of iodine with other compounds in the ceramics.

A possibility to directly and selectively investigate the distribution of lipids in the ceramic matrix is mass spectrometry imaging (MSI). In MSI, mass spectrometry data is acquired from individual points of a surface, thus creating data sets that allow visualisation of the precise distribution and location of compounds of interest. Although used on occasion in archaeological research (14, 15) it had not been applied to investigate absorbed lipid residues in archaeological ceramics. Here, we used a novel hybrid secondary ion mass spectrometry (SIMS) instrument equipped with a Time-of-Flight (ToF) and an Orbitrap mass analyser, known as a 3D OrbiSIMS (16), to investigate the distribution of lipids in wall cross sections of selected reference and archaeological samples with sub-micrometer spatial resolution (17). The higher acquisition speed of the ToF analyser allowed the imaging even of large areas several squaremillimetres in size within two hours while the higher spectral resolution and mass accuracy of the Orbitrap allowed confirmation of peak identities. Combined with scanning electron microscopy (SEM) and energy-dispersive X-ray spectroscopy (EDS) to further characterise the surface structure and composition, MSI could be used to gain direct and new insights in the distribution and preservation mechanisms of lipids in archaeological pottery.

Results and discussion

Analysis of reference lipids and modern replica pottery

Lipids of interest (free fatty acids, monoacylglycerols, diacylglycerols, and triacylglycerols) were initially dosed on the surface of aluminium foil (simple background) and blank modern replica ceramics with mass spectra subsequently acquired in positive and negative polarity (Figure S3). Analysis of the data suggested that the highest sensitivity for free fatty acids (the most common archaeological lipid) was achieved in negative mode, where palmitic acid (16:0) and stearic acid (18:0) were detected as $[M-H]^-$ ions at *m/z* 255.3 and 283.3, respectively. It is noteworthy that an intense signal at *m/z* 255.3 was also detected for acylglycerols containing palmitic acid, showing the value of this signal to be used as a proxy for lipids in archaeological samples. In positive polarity, free fatty acids were detected as $[M+H]^+$ and $[M-OH]^+$ ions, while triacylglycerols showed $[M-ROOH+H]^+$ fragment ions (Figure S3). The molecular ion was only detected with very low

abundance. Dosing the same compound on modern blank ceramics instead of aluminium foil did not impact the mass spectra of the lipids observed.

Using ToF-SIMS, lipids could be clearly detected in a 5 × 1.5 mm^2 analysis (Figure 1a,b) along the wall cross section of a modern reference ceramic pot which had been used to boil pork meat (uptake of ca 17 mg lipids per g ceramics, determined by gas chromatography-flame ionisation detection, GC-FID). In fact, fatty acid fragments corresponding to palmitic acid, stearic acid and oleic acid were among the most intense ions in the spectrum taken from the pot cross section (Figure 1a). From GC-FID analysis it was known that the principal lipids absorbed into the ceramics were triacylglycerols (C_{48}-C_{56}, maximum at C_{52}), and using ToF-SIMS in positive ionisation the respective $[M\text{-}ROOH+H]^+$ fragments could be detected (Figures S4 and S5). A significantly increased intensity of lipid signals was detected in the inner 2 – 3 mm of the wall (Figure 1c), indicating that the lipid permeation to the outer parts of the vessel was very limited in the current experiment comprising of only ten cooking steps (compared to possibly thousands in archaeological vessels). Further ToF-SIMS analysis undertaken at higher spatial resolution for smaller areas of interest, specifically 500 × 500 μm^2 and 100 × 100 μm^2 sections, revealed that the lipids were not evenly distributed but concentrated in defined zones (Figure S6). Confirmation of peak assignment was achieved using the Orbitrap mass analyser and a gas cluster ion beam (GCIB) where the respective ions for 16:0, 18:0 and 18:1 were detected at *m/z* 255.2333 ($C_{16}H_{31}O_2^-$, +1.5 ppm), *m/z* 283.2647 ($C_{18}H_{35}O_2^-$, +1.4 ppm) and *m/z* 281.2487 ($C_{18}H_{33}O_2^-$, +0.4 ppm), respectively.

Distribution of lipids in archaeological samples

Five selected archaeological samples (A1-A5) with known lipid contents (0.5 – 6.3 mg/g after solvent extraction, GC-FID) and compositions were selected and small subsamples were sectioned and prepared for SIMS analysis. Several sample areas of the cross sections (generally 500 × 500 μm^2 sections), situated towards the inside (i.e. close to the cooking goods), centre and outside of the wall were analysed in each sample to assess the presence of lipids and their spatial distribution. Clear lipid signals could be detected in all samples, but in different distributions and within features of different sizes (Figure 2, Figure S7). It has to be noted that SIMS analysis did not provide the same degree of information on molecular composition and lipid sources that is available through extraction and subsequent analysis using established coupled chromatographic/mass spectrometry techniques, but instead provided information on the micrometer-precise spatial distribution with sub-monolayer sensitivity in the samples.

In all areas analysed the lipids observed were unevenly distributed and observed in distinct pockets, which were also characterised by low intensity or an absence of the O^- ion. The O^- ion was found uniformly distributed in the inorganic matrix, which was mainly aluminium silicate. The sizes of lipid accumulations varied widely, generally ranging from ca. 5 – 50 µm, although some were more than 200 µm in size (Figure 2a, Figure 3, Figure S7). Most likely, this represents connected larger cavities within the ceramic matrix created during firing from temper material or evaporation of gases and water (18, 19). Lipids tended to be more abundant in the sampled areas lying closer to the inside of the wall, but a bias from the manual selection of suitable sample areas has to be considered (i.e. not all areas were flat enough for analysis). The observation that lipids accumulate in areas as large as several hundred micrometers showed that in these samples it was not only individual nanometer-sized pores that supported lipid preservation, but rather more macroscopic areas and structures in the ceramic.

Archaeological sample A1, that only showed weak lipid-related ion intensities, in contrast showed intensive CN^- and OCN^- signals (*m/z* 26.0 and *m/z* 42.0), which are common in the SIMS spectra of proteins or their degradation products, i.e. smaller peptides or individual amino acids (20) (Figure 2b, Figure S7).

Archaeological sample A5 with macroscopic white inclusions in its structure, likely temper added to the clay during vessel production, was investigated in further detail (Figure 3) (21). Analysis of a 3 × 2 mm^2 area of the wall cross section revealed a large accumulation of lipids (ca. 400 µm × 100 µm ellipsoid) present directly on one of the white inclusions and this was the largest lipid accumulation in all investigated samples. Further data from ToF-SIMS analysis (negative and positive ionisation) and EDS revealed that, while the surrounding matrix was rich in aluminium and silicon (which was expected from a clay), the inclusion was rich in calcium, carbon and oxygen, therefore identified as calcium carbonate (Figure 3, Figure S8). Furthermore, SIMS revealed large accumulations of lipids on a second macroscopic calcium carbonate inclusion in the same sample (Figure S9). In contrast, lipids were less frequently detected by SIMS in areas outside of the inclusions.

Association of fatty acids to calcium carbonate

Calcium carbonate is a common temper material in archaeological ceramics, often originating from shells or limestone (22). An explanation for the accumulation of lipids on this specific spot can be found in the calcium fatty acid salts, which are practically insoluble in water (K_{SP} of calcium dipalmitate is 10^{-17} mol^3/L^3) (23). Any traces of free fatty acids, dissolved in water, would gradually precipitate with traces of dissolved Ca^{2+} present on the surface of calcium carbonate, forming over centuries and millennia insoluble agglomerations. This formation of calcium fatty acid salts from calcium carbonate under excess of saturated fatty acids has been observed in previous studies (24). In addition, experimental work with geological reference material indicated a strong adsorption of fatty acids to calcium carbonate surfaces (25). In archaeological samples this preservation of lipids as calcium fatty acid salts would be a secondary process, because fatty acids have to be liberated from triacylglycerols and other ester lipids first. Furthermore, the ceramics need to show sufficient porosity and permeability to allow the dissolved fatty acids to reach the calcium-rich inclusions. Unfortunately, in our samples SIMS did not allow the reliable differentiation between free fatty acid, intact triacylglycerol and the calcium salt. Similarly, while this differentiation is achievable using micro Fourier-transform infrared spectroscopy (26), in our case the sensitivity was insufficient to yield unequivocal data from the archaeological samples.

This entrapment of fatty acids as calcium salts has several important implications for archaeological research. Primarily, it represents a second independent lipid preservation mechanism in addition to the assumed mechanism of lipid preservation through passive adsorption onto the ceramic surfaces. A precipitation as calcium salts protects the fatty acids effectively from ground water leaching and might reduce their availability as carbon source for the microbial community. Furthermore, the presence of calcium fatty acid salts could explain differences in lipid yields using two commonly used lipid extraction strategies. Compared to extractions using chloroform/methanol 2:1 (*v/v*) a combined extraction/methylation of lipids using sulfuric acid in methanol was found to frequently yield significantly higher lipid contents (8). The calcium salts of fatty acids would be insoluble in organic solvents, while acidic conditions would lead to a protonation of the fatty acids and a dissociation of the salts, thus allowing the fatty acids to be extracted using organic solvents and yielding higher quantities of lipids. In agreement with this, a recent study reported the analysis of lipids in nine calcified deposits from ceramic vessels. While solvent extraction yielded quantifiable lipid contents only in one sample, lipids could be recovered in significant quantities from all nine samples using a combined acid-based extraction/methylation approach (27).

To further assess the difference in performance of both extraction methods, ceramic powder of sub-samples from archaeological sample A5 and 19 further archaeological samples were split, and lipids were extracted using both methods. As anticipated, sulfuric acid/methanol extracted

more lipids in 15 samples, but this increase varied between threefold and 55-fold higher yields, with sample A5 yielding 47 000 µg/g more using the acidified methanol protocol (Table 1). In fact, in the sample with highest relative increase (14-6), EDS revealed similar calcium carbonate inclusions. On the other hand, in the sample with the second highest increase (21-1), calcium was more evenly distributed in the matrix, and the same was true for a sample with no increase between both methods (15-10). However, the difference between these samples was lower content of carbon in the latter, which suggests that the calcium might not be bound as carbonate (Supporting Information, Figures S10– S12).

Discussion and conclusions:

Preserved lipids, i.e. C_{16} and C_{18} fatty acids, in archaeological ceramics could be directly detected and their distributions visualised for the first-time using SIMS. The lipids were found concentrated in zones of generally 5 - 50 µm size, although some exceeded 200 µm. This showed that rather than nanometer-sized pores, more macroscopic structures were involved in facilitating lipid preservation. Future applications of spatially-resolved lipid analysis in pottery could address in more detail how different food processing techniques (e.g. water boiling vs. roasting) could lead to differences in the permeation depth and distribution patterns of lipids in the fabric (as seen in Figure 1) and offer a means to derive additional cooking technology-related information alongside compositional information from absorbed lipid residues. Critically, this could be achieved using a single sherd instead of requiring the rare case that multiple samples from the same vessel along the vertical profile are available for analysis (Charters, et al., 1993, Charters, et al., 1997). Furthermore, this technique finally offers a direct means of probing how pottery technology, e.g. raw material, temper and firing conditions, and consequential differences in properties such as porosity and pore connectivity, impact the capability of the ceramics to absorb and preserve lipids. A better understanding of these factors enables archaeological scientists to select samples for analysis that have the highest chances of yielding interpretable quantities of lipids, thus limiting the sampling and destruction of precious samples that ultimately do not offer any information. This would also lead to significant improvements in the quality of interpretations, since the quantitative differences in lipids recovered due to differences in the lipid preservation capabilities of ceramics can be disentangled from those resulting from the actual history of use. Finally, creating a benchmark for distributions of lipids in archaeological pottery would offer a means to unequivocally identify extraneous, modern lipid contaminations through different distribution patterns and thus address one of the major and ever present issues in ORA.

The data in this study also indicate that the precipitation of fatty acids as calcium salts on calcium-rich inclusions contributes to lipid preservation. In addition to providing first hints of this hitherto not considered mechanism of lipid preservation, the presence of calcium fatty acid salts needs to be considered during selection of extraction conditions, as solvent extraction will not allow the recovery of these lipid species. This work demonstrates how (in some samples) acid extraction can yield more than fifty-fold higher lipid contents compared to solvent extraction. In particular where carbonate-rich pottery fabrics or tempers, e.g. Shelly Ware, are being analysed, acid extraction should be the method of choice, potentially with parallel solvent extraction of a portion of the powdered sample.

In summary, these findings have implications in two key areas of organic residue research. Firstly, this new understanding of the mechanisms of lipid uptake and preservation will refine existing methodologies to ensure most effective sampling and analysis of irreplaceable archaeological material. Namely, this will (i) guide in the selection of most likely fabrics/tempers to preserve highest quantities of lipid (ii) guide in the most effective extraction methodology to release lipids from the pottery fabric and (iii) help understand and control for quantitative differences in lipid amounts due to the propensity of ceramic fabrics to preserve lipid, allowing inferences about historic use to be constructed. Secondly, future research in this field has the potential to unlock further information of archaeological relevance encapsulated in the preserved lipids, with possibilities existing to explore methods of historic use, and extraneous contamination, based on visualization of the spatial distribution of lipids. This will ensure that the maximum amount of information can be drawn from every archaeological potsherd, which is crucial since not only is ORA a labour-intensive and expensive approach on the scale it is usually applied, but, most importantly, unique archaeological samples will be destroyed and re-analysis is often impossible.

Materials and Methods

Samples

Archaeological samples from Vindolanda (UK, ca. 105-120 CE), Kingscote (UK, 4th century CE) and Oxford (UK, 10th - 13th century CE) were selected based on their abundant lipid contents found in previous analyses. Additional information about the samples and the sites is available in the Supplementary Information (Table S1, Figure S1 and S2). All samples were sherds from the rim of the vessels, as these tend to yield the highest lipid contents (28, 29). Modern replica pots (ca. 10 cm high, 10 cm diameter, 1 cm wall thickness, 500 mL volume) was produced from a clay/sand mixture (3:1, w/w) and fired under 1000 ºC (The Pot Shop, Lincoln, UK). After firing and cooling down, the replica pots were immediately wrapped in paper and subsequently only handled wearing nitrile gloves. Archaeological samples were stored wrapped in aluminium foil and only handled wearing nitrile gloves at all times to avoid contamination.

Analysis of lipids by GC-FID and GC-MS

Subsamples of pot sherds were cleaned using a model drill and lipids were extracted and analysed as described before (3). In short, 1-2 g of powdered ceramics were extracted using chloroform/methanol 2:1 (*v/v*) under sonication, filtered over silica and analysed after trimethylsilylation by high temperature GC-FID and GC-MS (3). Alternatively, samples were extracted and transesterified using sulfuric acid in methanol prior to GC-FID and GC-MS analysis as described earlier (8).

Preparation of samples for SIMS

Just before SIMS analysis, subsamples (roughly 1 × 1 × 1 cm^3) from archaeological and modern replica pot sherds (taken from the area below the rim) were produced using a hammer and a chisel wearing nitrile gloves, which were changed between samples. The chisel was cleaned using HPLC grade dichloromethane and 2-propanol between samples. The cross sections were smoothed using fresh P240 and P600 sandpaper (average particle diameters of 58.5 µm and 25.8 µm, respectively) until visibly plane. Initially, test samples were also prepared without sandpaper smoothing and using a diamond-coated tile cutting disc instead of a hammer and chisel to separate the subsamples. However, sandpaper-treated samples showed to be best suitable for SIMS analysis and accordingly all samples were subsequently prepared using a hammer and chisel and included sandpaper smoothing. A blank replica pot sample was prepared identical to the samples and no lipids were detected in this sample using SIMS.

Analysis of samples by Secondary Ion Mass Spectrometry

Reference solutions of lipids (palmitic acid, 1,2-dipalmitoyl-glycerol, tripalmitate) were dosed on clean aluminium foil and surface of blank ceramic fragments to collect reference spectra. Analysis were performed using a ToF-SIMS with Orbitrap functionality (Hybrid SIMS (IONTOF GmbH, prototype developed as "3D OrbiSIMS"). Chemical imaging was performed employing a liquid ion gun with a Bi_3^+ primary ion source operated at 30 keV (and a target current of 0.03 pA) employing a ToF analyser (mode 6 (16)) in delayed extraction analysis configuration. Macroscale analysis was conducted for 5 × 1.5 mm^2 and 2.5 × 3 mm^2 areas at a pixel resolution of 100 pixels per mm. Microscale analysis was performed over 500 × 500 μm^2 and 100 × 100 μm^2 areas at a pixel resolution of 256 × 256. An Ar_{2300}^+ GCIB operated at 20 keV (target current of 220 pA) was used with the Orbitrap mass analyser in a depth profiling functionality (mode 4 (16)). In negative and positive ionisation data were recorded from *m/z* 1-550 and *m/z* 1-1000, respectively. In order to provide charge compensation for the non-conductive sample a low energy electron floodgun was applied throughout.

Scanning Electron Microscopy and energy-dispersive X-ray spectroscopy analysis

A Jeol JSM-IT300 (Tokyo, Japan) instrument operated at 15 kV was used to acquire scanning electron micrographs using secondary and backscattered electron detectors at 50-1500x magnification. The instrument was also equipped with an X-Max 80 mm^2 EDS detector (Oxford instruments, Oxford, UK) for EDS measurements.

Data availability

The SIMS data generated during the current study are available at the Radar data repository (https://www.radar-service.eu) at doi: 10.22000/318

Competing interests:

The authors have no competing interests.

Acknowledgments: This research was supported by the Gerda-Henkel Foundation (AZ 27/V/18) and the University of Bristol's School of Arts and Faculty of Arts Research Funds. The Engineering and Physical Sciences Research Council (EPSRC) are gratefully acknowledged for the Strategic Equipment grant '3D OrbiSIMS: Label free chemical imaging of materials, cells and tissues' funding that supported this work (grant no. EP/P029868/1). The authors thank Dr. Andrew Birley (Vindolanda Trust), Dr. Richard Madgwick (University of Cardiff) and John Cotter (Oxford Archaeology) for providing access to archaeological samples. The authors gratefully acknowledge the support of Dr. Jean-Charles Eloi (Chemical Imaging Facility, University of Bristol) for help with SEM and EDS measurements and of Caitlin Greenwood (University of Bristol) and Matti Froning (University of Münster) for assistance with lab procedures.

References

1. R. P. Evershed, Organic Residue Analysis in Archaeology: The Archaeological Biomarker Revolution. *Archaeometry* **50**, 895-924 (2008).
2. R. P. Evershed, Experimental approaches to the interpretation of absorbed organic residues in archaeological ceramics. *World Archaeol.* **40**, 26-47 (2008).
3. S. Hammann, L. J. E. Cramp, Towards the detection of dietary cereal processing through absorbed lipid biomarkers in archaeological pottery. *J. Archaeol. Sci.* **93**, 74-81 (2018).
4. M. Roffet-Salque *et al.*, Widespread exploitation of the honeybee by early Neolithic farmers. *Nature* **527**, 226-230 (2015).
5. J. Dunne *et al.*, First dairying in green Saharan Africa in the fifth millennium BC. *Nature* **486**, 390-394 (2012).
6. J. Dunne, A. M. Mercuri, R. P. Evershed, S. Bruni, S. di Lernia, Earliest direct evidence of plant processing in prehistoric Saharan pottery. *Nat. Plants* **3**, 16194 (2016).
7. R. P. Evershed *et al.*, Earliest date for milk use in the Near East and southeastern Europe linked to cattle herding. *Nature* **455**, 528-531 (2008).
8. M. Correa-Ascencio, R. P. Evershed, High throughput screening of organic residues in archaeological potsherds using direct acidified methanol extraction. *Anal. Methods* **6** (2014).
9. S. Hammann, L. J. E. Cramp, M. Whittle, R. P. Evershed, Cholesterol degradation in archaeological pottery mediated by fired clay and fatty acid pro-oxidants. *Tetrahedron Lett.* **59**, 4401-4404 (2018).
10. M. Regert, H. A. Bland, S. N. Dudd, P. v. Bergen, R. P. Evershed, Free and bound fatty acid oxidation products in archaeological ceramic vessels. *Proc. R. Soc. Lond. B Biol. Sci.* **265**, 2027-2032 (1998).
11. F. A. Hansel, M. S. Copley, L. A. S. Madureira, R. P. Evershed, Thermally produced ω-(o-alkylphenyl)alkanoic acids provide evidence for the processing of marine products in archaeological pottery vessels. *Tetrahedron Lett.* **45**, 2999-3002 (2004).
12. B. Stern, C. Heron, M. Serpico, J. Bourriau, A comparison of methods for establishing fatty acid concentration gradients across potsherds: a case study using Late Bronze Age Canaanite amphorae. *Archaeometry* **42**, 399-414 (2000).
13. L. Goldenberg, R. Neumann, S. Weiner, Microscale distribution and concentration of preserved organic molecules with carbon–carbon double bonds in archaeological ceramics: relevance to the field of residue analysis. *J. Archaeol. Sci.* **42**, 509-518 (2014).
14. V. Mazel, P. Richardin, "ToF-SIMS Study of Organic Materials in Cultural Heritage: Identification and Chemical Imaging" in Organic mass spectrometry in art and archaeology, M. P. Colombini, F. Modugno, Eds. (John Wiley & Sons, Ltd, 2009), pp. 433-457.
15. V. Mazel *et al.*, The patinas of the Dogon–Tellem statuary: A new vision through physico-chemical analyses. *J. Cult. Herit.* **9**, 347-353 (2008).
16. M. K. Passarelli *et al.*, The 3D OrbiSIMS—label-free metabolic imaging with subcellular lateral resolution and high mass-resolving power. *Nat. Methods* **14**, 1175 (2017).
17. M. K. Passarelli, N. Winograd, Lipid imaging with time-of-flight secondary ion mass spectrometry (ToF-SIMS). *Biochim. Biophys. Acta* **1811**, 976-990 (2011).

18. V. Kilikoglou, G. Vekinis, Y. Maniatis, P. Day, Mechanical performance of quartz-tempered ceramics: part I, strength and toughness. *Archaeometry* **40**, 261-279 (1998).
19. W.-A. Kahl, B. Ramminger, Non-destructive fabric analysis of prehistoric pottery using high-resolution X-ray microtomography: a pilot study on the late Mesolithic to Neolithic site Hamburg-Boberg. *J. Archaeol. Sci.* **39**, 2206-2219 (2012).
20. D. S. Mantus, B. D. Ratner, B. A. Carlson, J. F. Moulder, Static secondary ion mass spectrometry of adsorbed proteins. *Anal. Chem.* **65**, 1431-1438 (1993).
21. O. S. Rye, *Pottery technology: principles and reconstruction* (Taraxacum Washington, DC, 1981), vol. 4.
22. M. R. Bebber, L. B. Spurlock, M. Fisch, A performance-based evaluation of chemically similar (carbonate) tempers from Late Prehistoric (AD 1200-1700) Ohio: Implications for human selection and production of ceramic technology. *PloS one* **13**, e0194992 (2018).
23. R. Irani, C. Callis, Metal complexing of phosphorous compounds. II. Solubilites of calcium soaps of linear corboxylic acids. *J. Phys. Chem.* **64**, 1741-1743 (1960).
24. R. A. Berner, Calcium Carbonate Concretions Formed by the Decomposition of Organic Matter. *Science* **159**, 195-197 (1968).
25. G. C. Frye, M. M. Thomas, Adsorption of organic compounds on carbonate minerals: 2. Extraction of carboxylic acids from recent and ancient carbonates. *Chem. Geol.* **109**, 215-226 (1993).
26. V. Otero *et al.*, Characterisation of metal carboxylates by Raman and infrared spectroscopy in works of art. *J. Raman. Spectrosc.* **45**, 1197-1206 (2014).
27. J. Hendy *et al.*, Ancient proteins from ceramic vessels at Catalhoyuk West reveal the hidden cuisine of early farmers. *Nat. Commun.* **9**, 4064 (2018).
28. S. Charters *et al.*, Quantification and distribution of lipid in archaeological ceramics: implications for sampling potsherds for organic residue analysis and the classification of vessel use. *Archaeometry* **35**, 211-223 (1993).
29. S. Charters, R. P. Evershed, A. Quye, P. W. Blinkhorn, V. Reeves, Simulation experiments for determining the use of ancient pottery vessels: the behaviour of epicuticular leaf wax during boiling of a leafy vegetable. *J. Archaeol. Sci.* **24**, 1-7 (1997).

Figures and captions to Figures

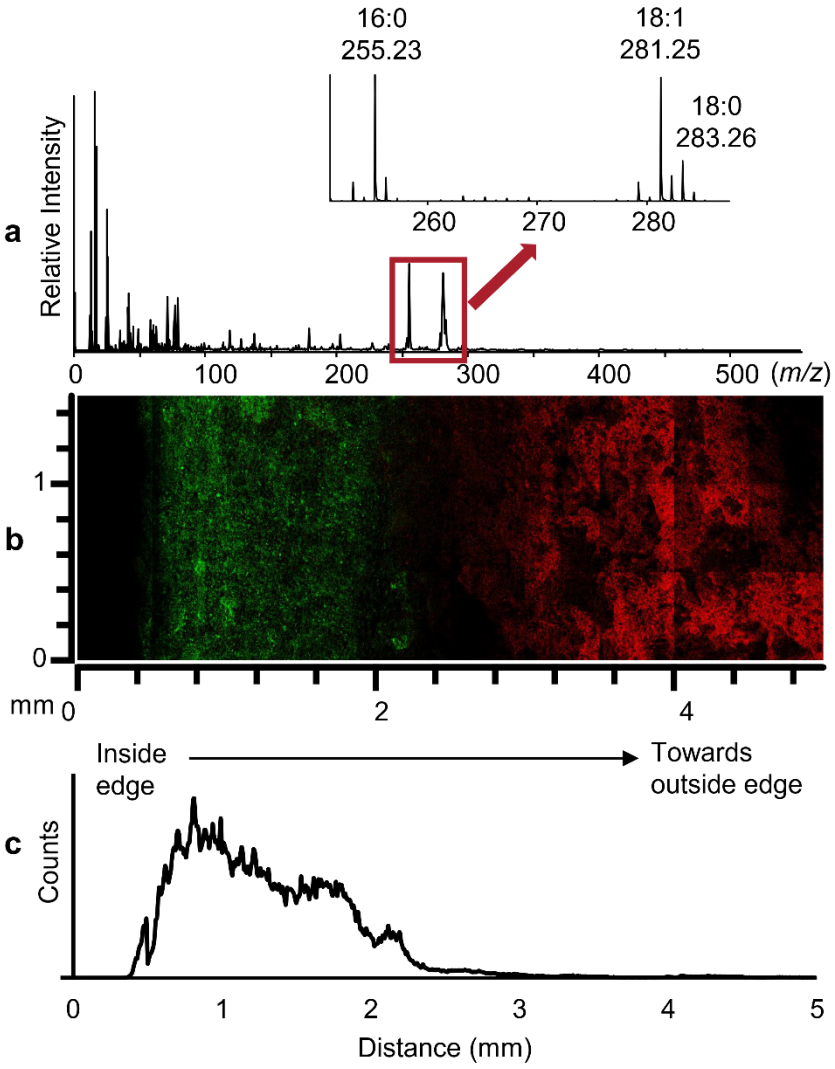

Figure 1. Analysis of lipid distributions in a reference ceramic sample using ToF-SIMS a: ToF-SIMS spectrum of the reference sample (replica pot used to cook pork meat) in negative ionisation mode with insert showing the mass region from *m/z* 250 to 290 where the $[M_{FA}\text{-}H]^-$ ions of lipids were detected. b: Overlay of lipid signals ($C_{16}H_{31}O_2^-$, $C_{18}H_{33}O_2^-$ and $C_{18}H_{35}O_2^-$, green) and a matrix signal (O^-, red) over a 1.5 × 5 mm^2 ToF-SIMS analysis of the wall cross section from the inside edge (left) to the outside (right) showing the accumulation of lipids in the inner 2 mm of the sample. Brighter colour denotes higher intensity. c: Intensity profile of lipid signals (sum of intensities of $C_{16}H_{31}O_2^-$, $C_{18}H_{33}O_2^-$ and $C_{18}H_{35}O_2^-$) through the cross section again showing the accumulation of lipids towards the inside edge.

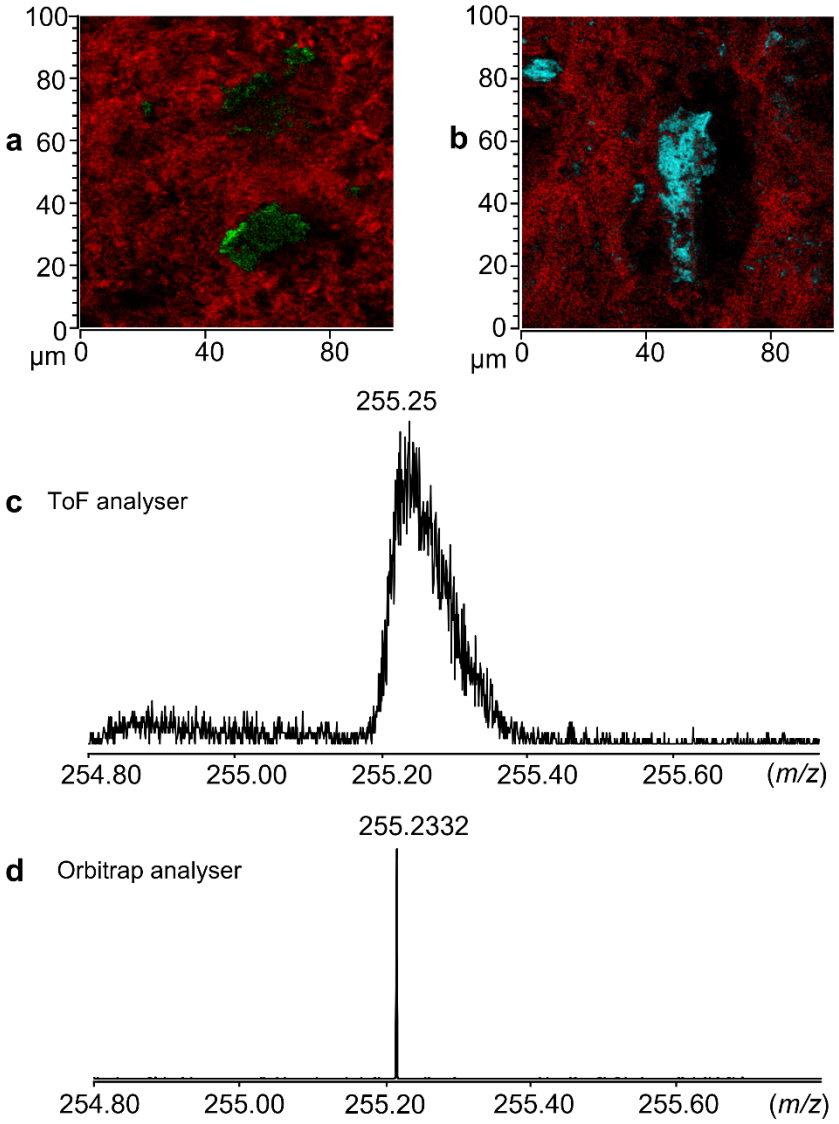

Figure 2: **Analysis of archaeological ceramics**. (a): ToF-SIMS image of the wall cross section of archaeological sample A3, overlay of lipid signals ($C_{16}H_{31}O_2^-$, $C_{18}H_{33}O_2^-$ and $C_{18}H_{35}O_2^-$, green) and a matrix signal (O^-, red) for a 100 × 100 μm^2 section (b): ToF-SIMS image of the wall cross section of archaeological sample A1, overlay of CN^-/OCN^- (*m/z* 26.0 and *m/z* 42.0) signals, common in SIMS spectra of proteins, (blue) and a matrix signal (O^-, red) for a 100 × 100 μm^2 section indicating the presence of nitrogen-containing organic compounds. Pixel size in both ion maps is 0.5 μm. (c,d) SIMS spectra of the area shown in a using the ToF and Orbitrap mass analyser in the mass range from *m/z* 254.8 to 255.8 showing the $[M-H]^-$ ion of palmitic acid ($C_{16}H_{31}O_2^-$, *m/z* 255.2324), demonstrating the superior resolution and mass accuracy of the Orbitrap mass analyser.

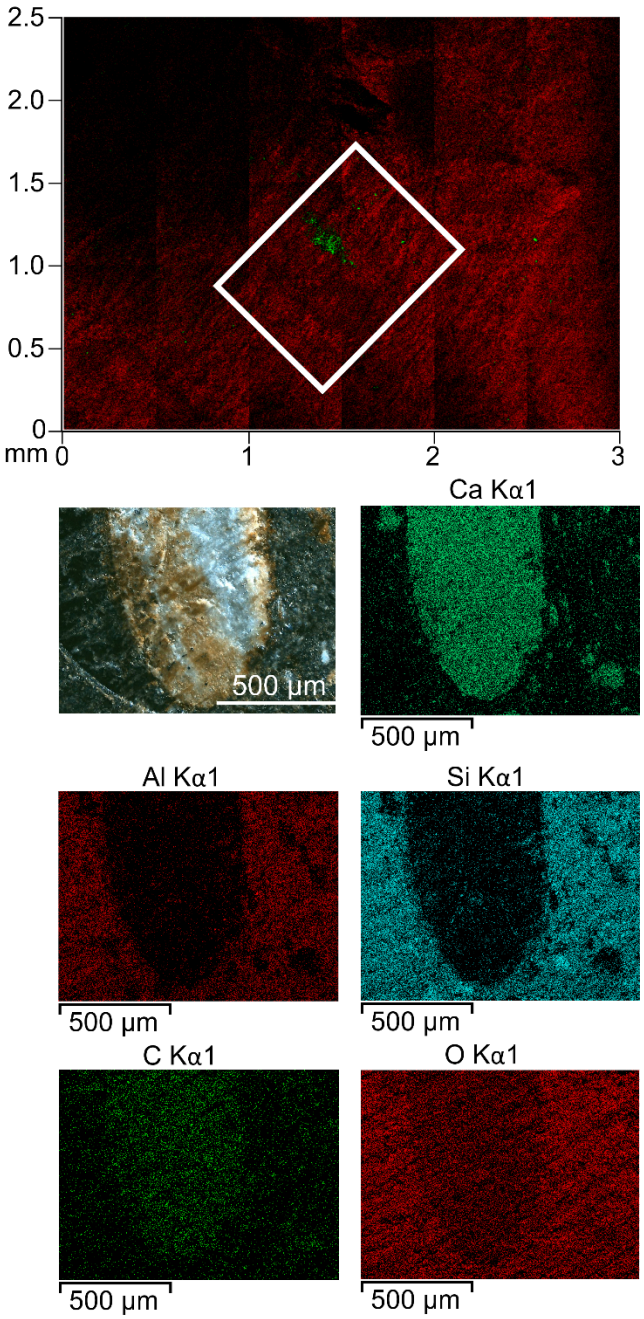

Figure 3: **Analysis of an archaeological ceramic sample by ToF-SIMS and energy-dispersive X-ray spectroscopy (EDS).** Top: ToF-SIMS image of the wall cross section of archaeological sample A3, overlay of lipid signals ($C_{16}H_{31}O_2^-$, $C_{18}H_{33}O_2^-$ and $C_{18}H_{35}O_2^-$, green) and a matrix signal (O^-, red) for a 3 × 2.5 mm^2 area and a photographic image of the area marked in white as well as SEM-EDS images of Ca, Al, Si, C, and O of this area with the white inclusion and the surrounding ceramic matrix. Brighter colour denotes higher intensity.

Tables

Table 1: Lipid yields for samples analysed using solvent extraction ($CHCl_3$/MeOH 2:1 (*v/v*)) and sulfuric acid in methanol, as well as absolute and relative difference (yield using sulfuric acid/methanol divided by yield using solvent extraction). Samples marked in bold were also analysed by SEM-EDS (Supplementary Information, Figures S10-S12)

Sample Name	Lipid yield solvent extraction (µg/g)	Lipid yield sulfuric acid/methanol (µg/g)	Difference absolute (µg/g)	Difference relative
A5	6260	53380	47120	8.5
1-7	24	508	484	21.2
1-11	54	774	720	14.3
1-16	242	1403	1161	5.8
2-1	318	941	623	3.0
3-5	13	146	133	11.2
3-6	338	1843	1505	5.5
5-3	<5	<5	n/a	n/a
6-2	<5	<5	n/a	n/a
13-2	34	89	55	2.6
14-6	45	2486	2441	55.2
15-4	51	440	389	8.6
15-6	582	4265	3683	7.3
15-10	137	61	-76	0.4
16-6	54	881	827	16.3
17-4	<5	94	94	n/a
19-3	<5	<5	n/a	n/a
20-1	<5	<5	n/a	n/a
21-1	1659	9410	7751	5.7
21-3	263	1145	882	4.4

PNAS
www.pnas.org

Supplementary Information for

Mechanisms of lipid preservation in archaeological clay ceramics revealed by mass spectrometry imaging

Simon Hammann[1,2 *], David J. Scurr[3], Morgan R. Alexander[3], Lucy J. E. Cramp[1]

[1] Department of Anthropology and Archaeology, University of Bristol, Bristol BS8 1UU, United Kingdom

[2] Department of Chemistry and Pharmacy, Friedrich-Alexander University Erlangen-Nürnberg, Nikolaus-Fiebiger Straße 10, 91058 Erlangen, Germany

[3] Advanced Materials and Healthcare Technologies, School of Pharmacy, University of Nottingham, Nottingham NG7 2TQ, United Kingdom

*corresponding author:

Simon Hammann
Friedrich-Alexander University Erlangen-Nürnberg
Nikolaus-Fiebiger Straße 10
91058 Erlangen, Germany
Email: simon.hammann@fau.de
Phone: +49 9131 8565391

This PDF file includes:

Table S1: Information about the samples, their context and results from previous analysis.

Sample	Site (site code)	Context	Date	Vessel form and sherd location	Fabric	Height and diameter	Lipid content (µg/g)	Stable carbon isotope data (‰)	Identification of lipid sources	Reference
A1	Queen's College, Oxford, UK (OXQCNG[1])	(355)	1050-1250 CE	Jar, rim	Late Saxon Oxford ware (OXY)	Unknown	510	$\delta^{13}C_{16:0}$: -28.2 $\delta^{13}C_{18:0}$: -29.8	Ruminant adipose fat	Fabric series: Mellor, M. 1994, A synthesis of middle and late Saxon, medieval and early post-medieval pottery from the Oxford region, Oxoniensia LIX, 17–218.[3]
A2	Praetorium of period IV fort, Vindolanda, UK	VY-27, courtyard of the praetorium	105-120 CE	Bowl, rim	Pre-hadrianic coarse ware	H: 4 cm D: 10 cm (estimated)	1590	$\delta^{13}C_{16:0}$:n/a $\delta^{13}C_{18:0}$: n/a	n/a	Background on excavation of the building: Birley, R,, 1994, Vindolanda. Research reports, New Series, Volume 1. The Early Wooden Forts. Roman Army Museum Publications, Greenhead. 113-127
A3	Schola in period IV fort, Vindolanda, UK	V01-04A, store room	105-120 CE	Bowl, rim	Pre-hadrianic coarse ware	H: 7 cm D: 15 cm (estimated)	2040	$\delta^{13}C_{16:0}$: -28.2 $\delta^{13}C_{18:0}$: -30.8	Ruminant adipose fat	Background on excavation of the building: Birley, R,, 1994, Vindolanda. Research reports, New Series, Volume 1. The Early Wooden Forts. Roman Army Museum Publications, Greenhead. 113-127
A4	Kingscote, UK (Kingscote Site 2)	Building VIII, Room 5 (47)	4th century CE	Jar, rim	Dorset Black Burnished Ware 1 (BB1)	Unknown	24530[2]	$\delta^{13}C_{16:0}$: -27.0 $\delta^{13}C_{18:0}$: -29.1	Mixed ruminant/non-ruminant adipose fats	Timby, J. ed. 1998. Excavations at Kingscote and Wycomb, Gloucestershire. Cirencester: Cotswold Archaeological Trust.
A5	St. Aldates, Oxford, UK (OXSTAD16[1])	(3078)	900-1050 CE	Jar, rim	Late Saxon Shelly Ware (OXB)	Unknown	6260	$\delta^{13}C_{16:0}$: -27.6 $\delta^{13}C_{18:0}$: -29.4	Ruminant adipose fat	Fabric series: Mellor, M. 1994, A synthesis of middle and late Saxon, medieval and early post-medieval pottery from the Oxford region, Oxoniensia LIX, 17–218.[3]

[1] Oxford Archaeology site code

[2] This sample was extracted using the sulfuric acid/methanol protocol, while the others were extracted using chloroform/methanol 2:1 (*v/v*)

[3] Publication of detailed reports on these sites is forthcoming in Oxoniensia

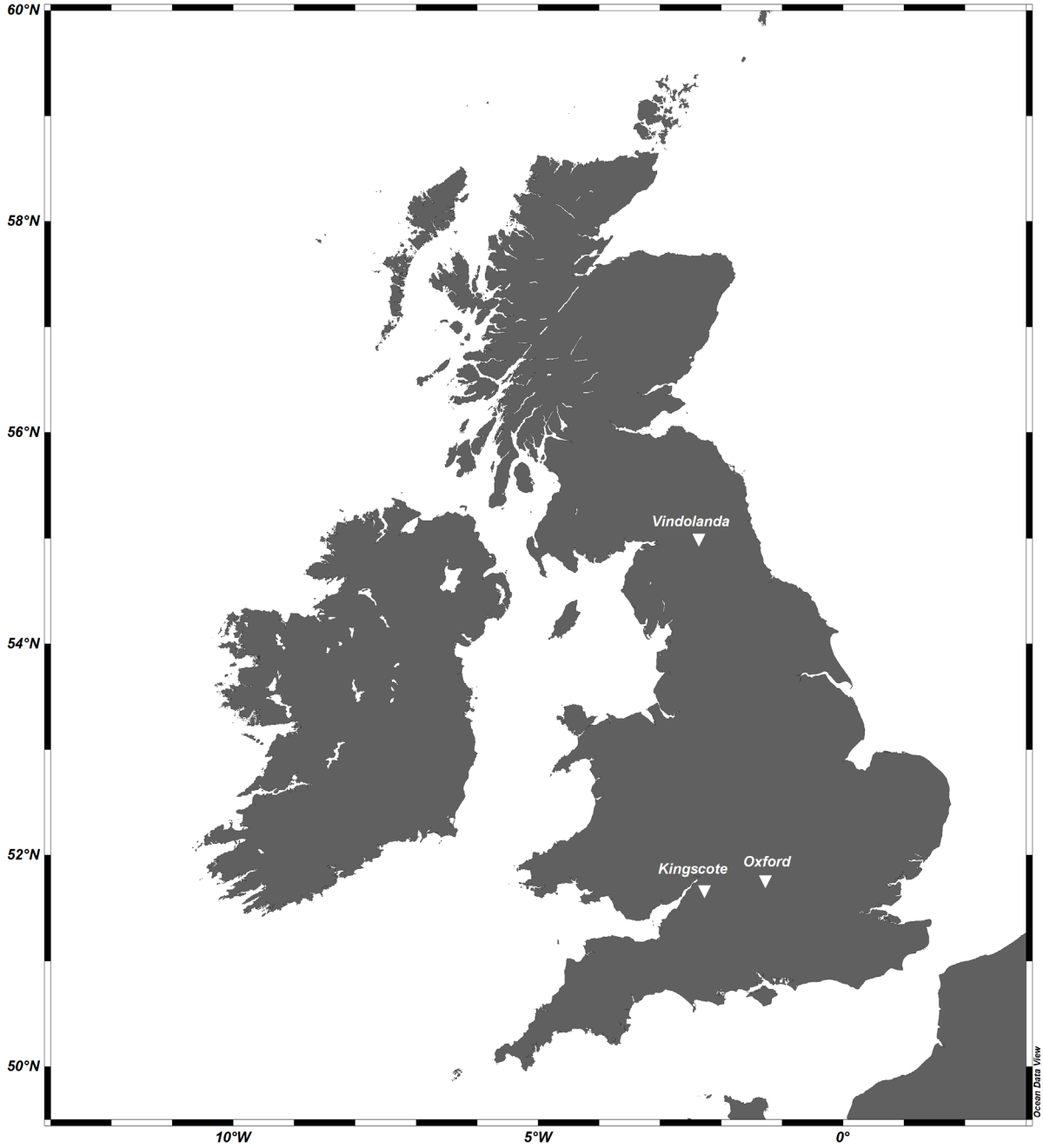

Figure S1: Map of Britain showing the location of Kingscote, Oxford and Vindolanda. The map was produced using Ocean Data View 5.2.1 (Schlitzer, Reiner, Ocean Data View, https://odv.awi.de, 2020)

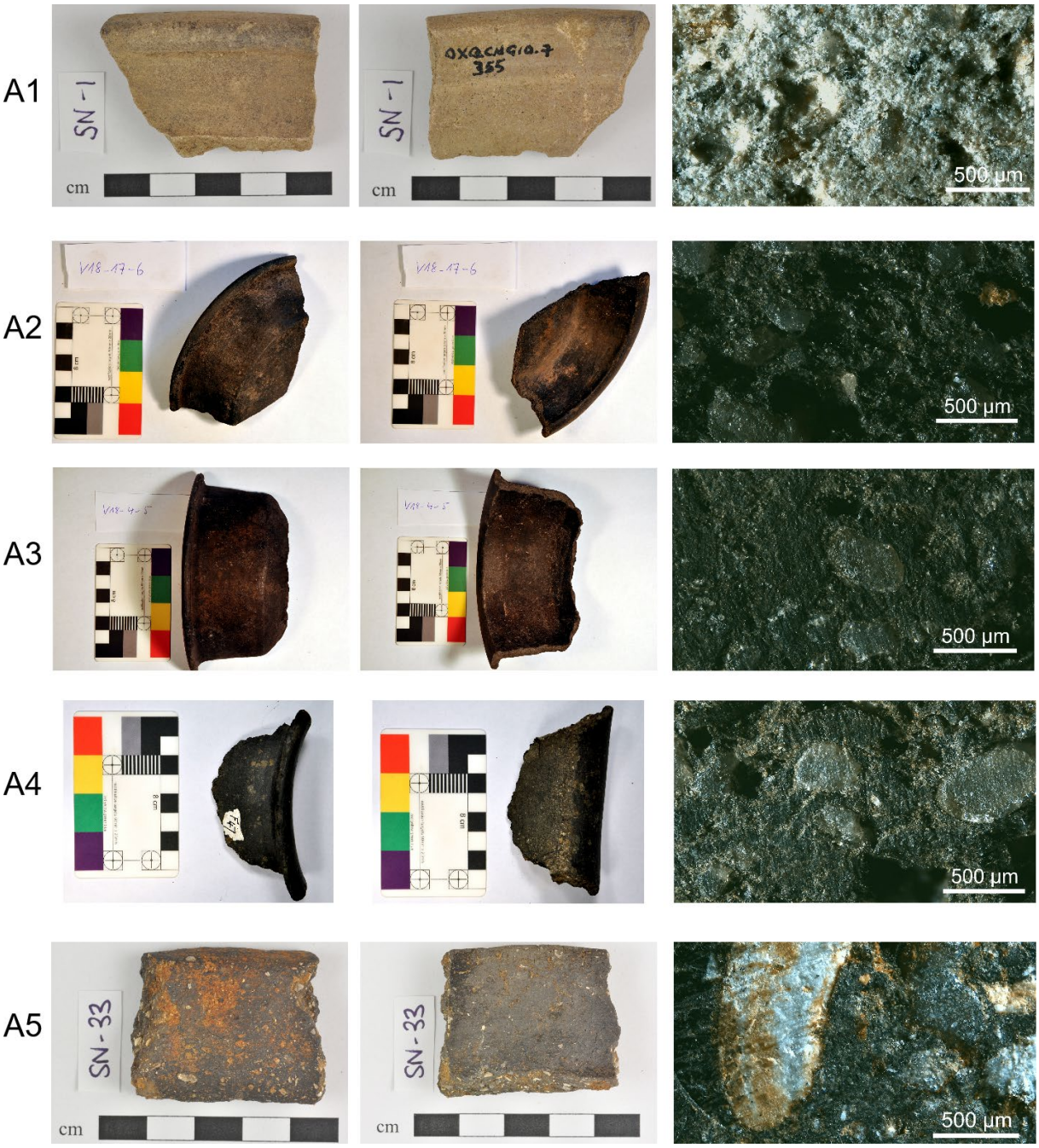

Figure S2: Photographic images of archaeological samples A1-A5 showing the sherd size and shape (left and middle column) as well as representative microscopic images of the wall cross sections (right column).

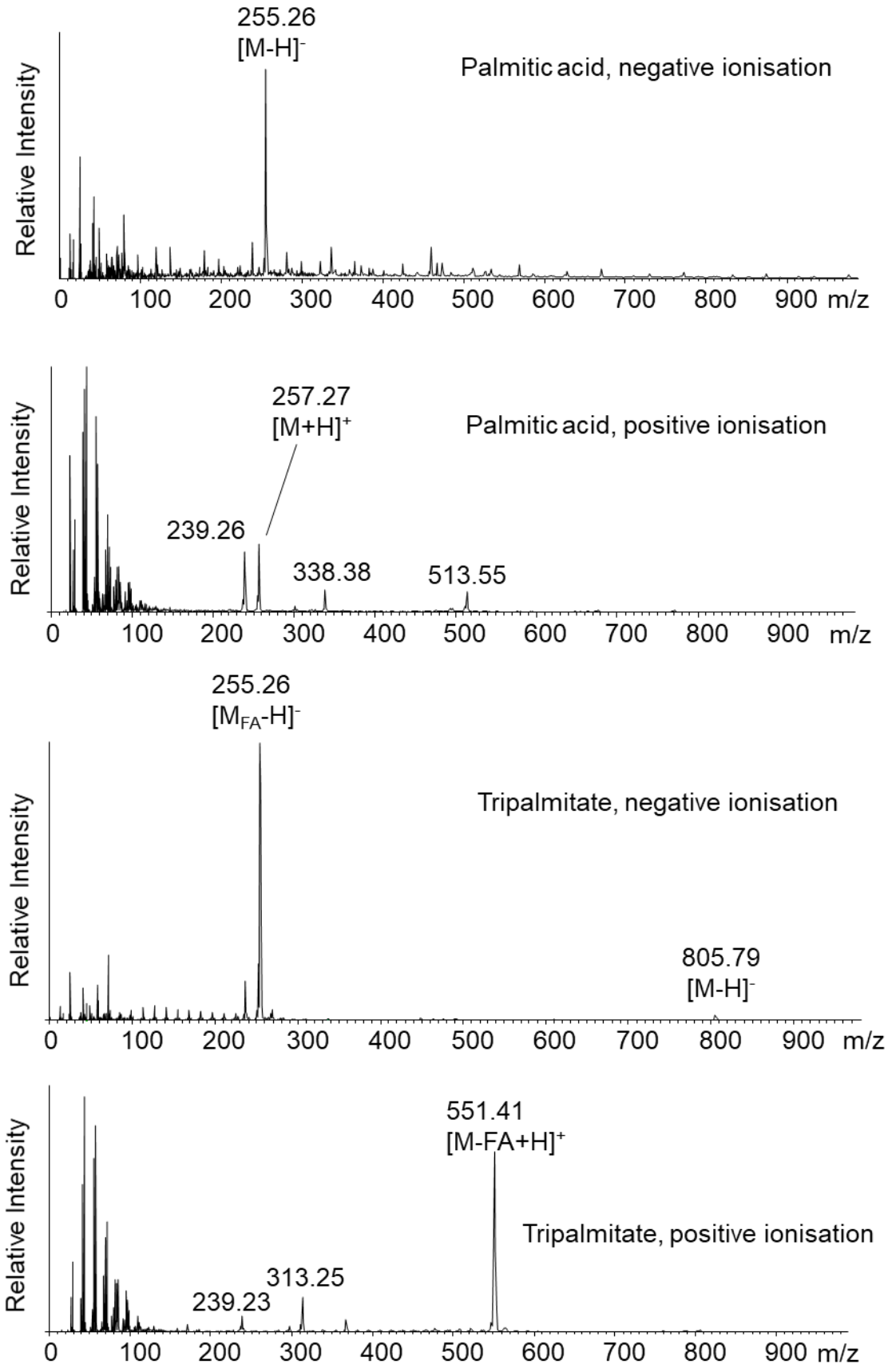

Figure S3: ToF-SIMS spectra of palmitic acid and tripalmitate standards dosed on aluminium foil in negative and positive ionisation

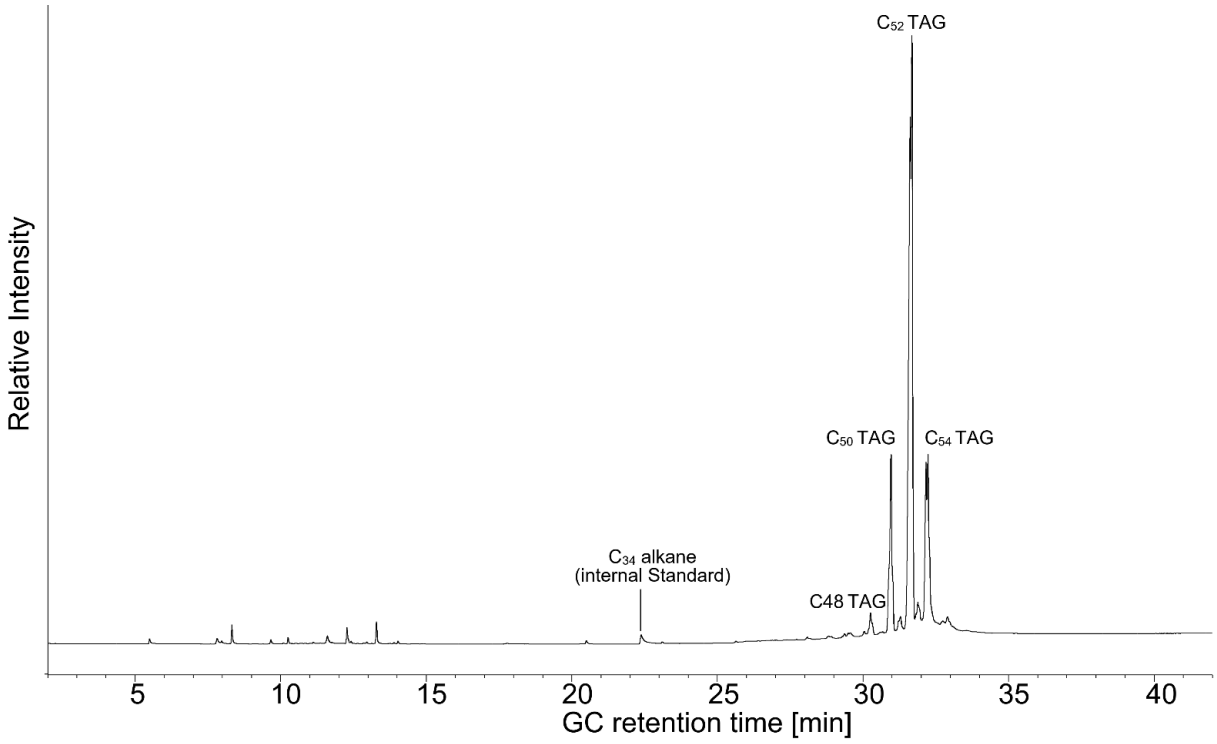

Figure S4: GC-FID chromatogram of a trimethlylsilylated lipid extract of the reference pot used to cook pork in the laboratory showing the absorption of lipids into the ceramics (17 mg/g) and dominance of C_{48}-C_{54}) triacylglycerols in the lipid pattern. The numbers denote the total carbon number of the fatty acid chains

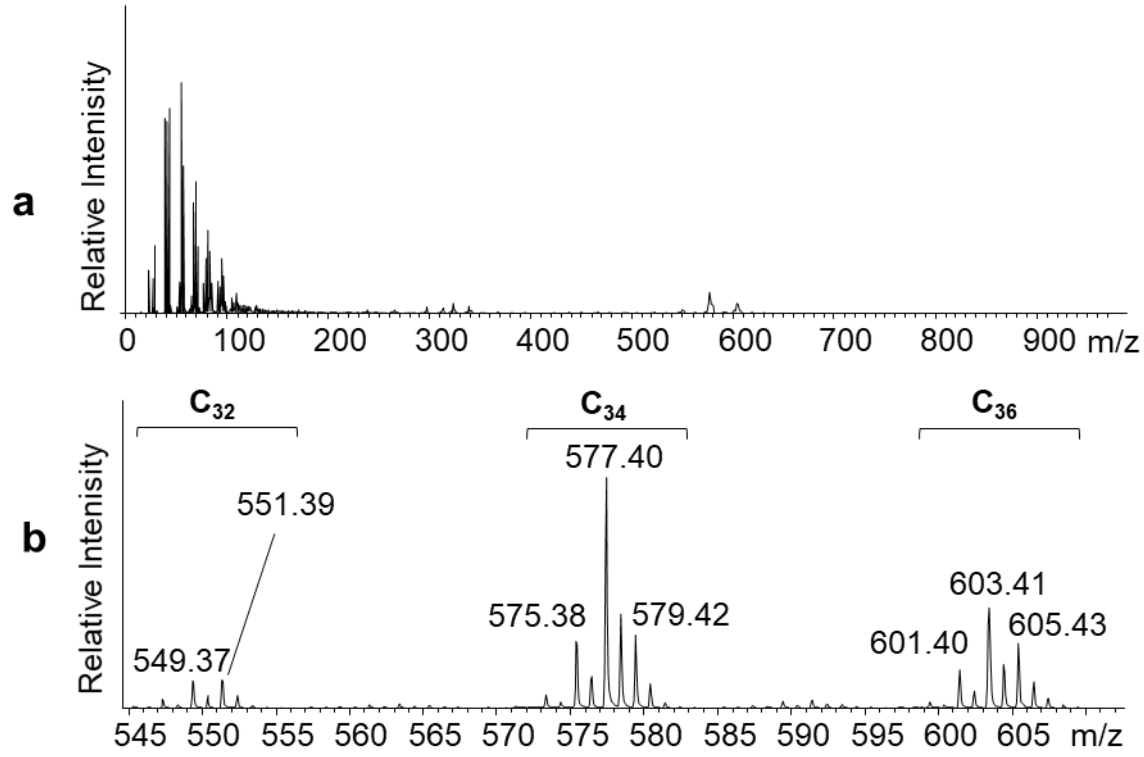

Figure S5: ToF-SIMS spectrum of the reference sample (replica pot used to cook pork meat) in positive ionisation mode (a) and enlarged the mass range from *m/z* 545 to 610 (b) where the C_{32}, C_{34} and C_{36} (sum of carbon atoms in the fatty acid chains) $[M\text{-}ROOH+H]^+$ diacylglycerol fragment ions of the triacylglycerols are detected (b).

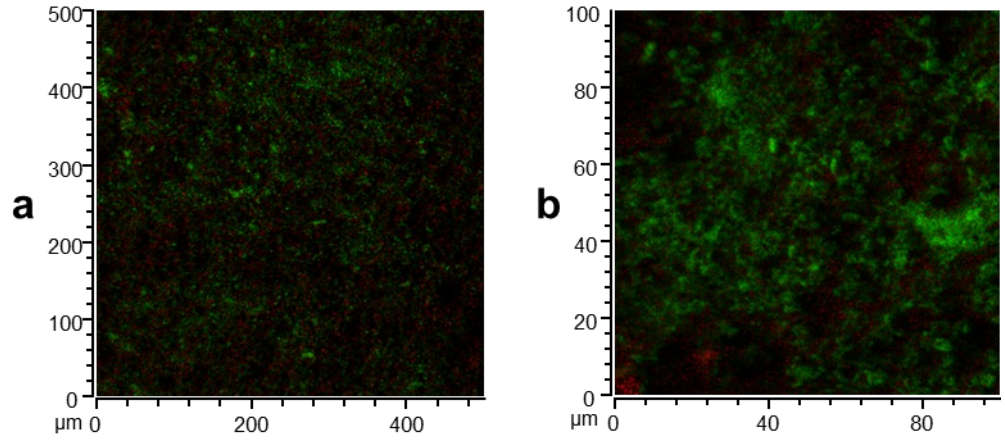

Figure S6: Overlay of lipid signals ($C_{16}H_{31}O_2^-$, $C_{18}H_{33}O_2^-$ and $C_{18}H_{35}O_2^-$, green) and a matrix signal (O^-, red) for 500 µm × 500 µm (a) and 100 µm × 100 µm (b) of the ToF-SIMS analysis of sections of the modern reference sample shown in Figure 1 acquired with higher spatial resolution. Brighter colours denote higher intensity.

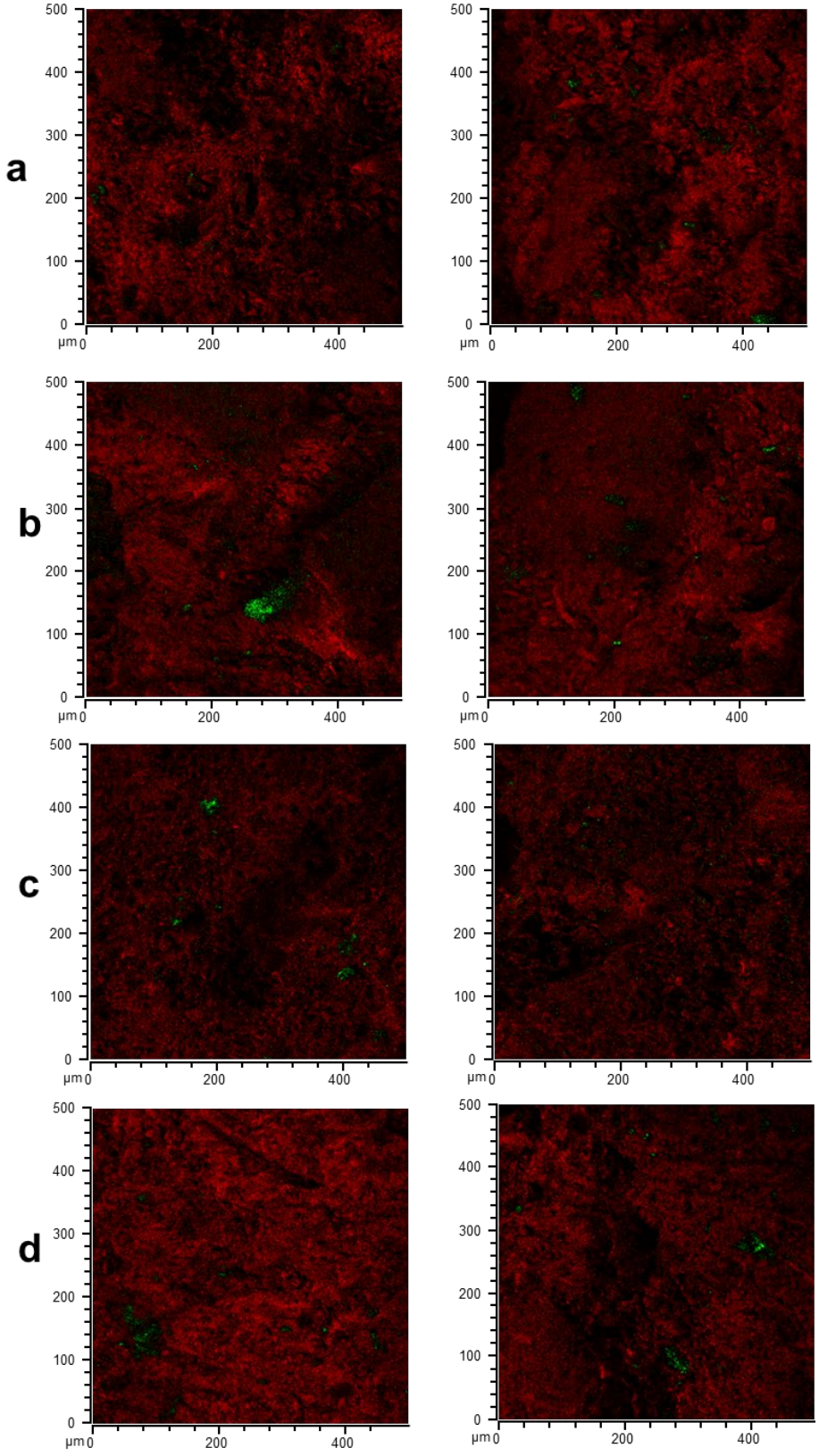

Figure S7: a): ToF-SIMS image of the wall cross sections of archaeological samples A1-A4 (a-d), overlay of lipid signals ($C_{16}H_{31}O_2^-$, $C_{18}H_{33}O_2^-$ and $C_{18}H_{35}O_2^-$, green) and a matrix signal (O^-, red) for 500 µm × 500 µm sections. The ion maps in the left and middle columns were acquired close to the inside and outside edge of the wall cross section, respectively.

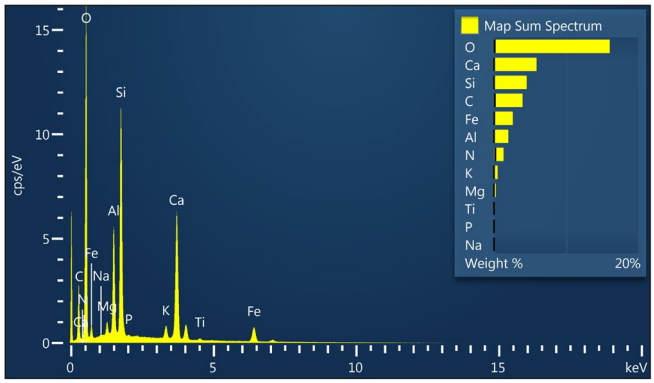

Figure S8: EDS spectrum of sample A5. The individual intensity maps are shown in Figure 3.

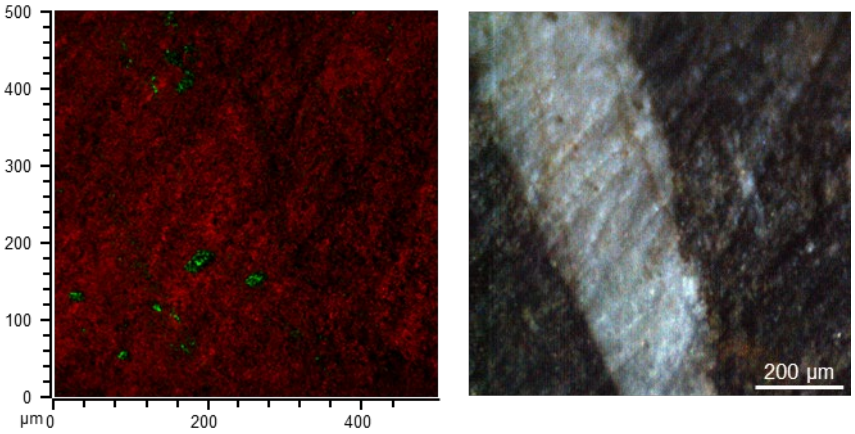

Figure S9: Left: ToF-SIMS image of the wall cross section of archaeological sample A5 , overlay of lipid signals ($C_{16}H_{31}O_2^-$, $C_{18}H_{33}O_2^-$ and $C_{18}H_{35}O_2^-$, green) and a matrix signal (O^-, red) for a 500 µm × 500 µm section. Right: photograph of the same area showing the white calcium carbonate inclusion.

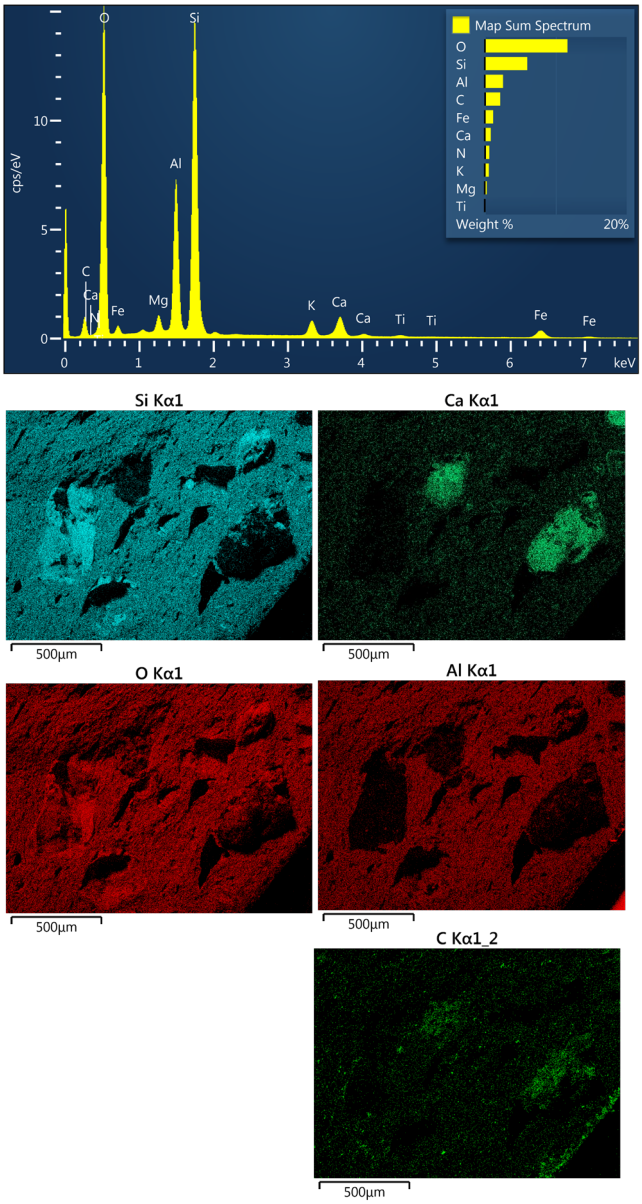

Figure S10: EDS spectrum of sample 14-6 and intensity maps for Si, Ca, O, Al and C. Brighter colour denote higher intensity.

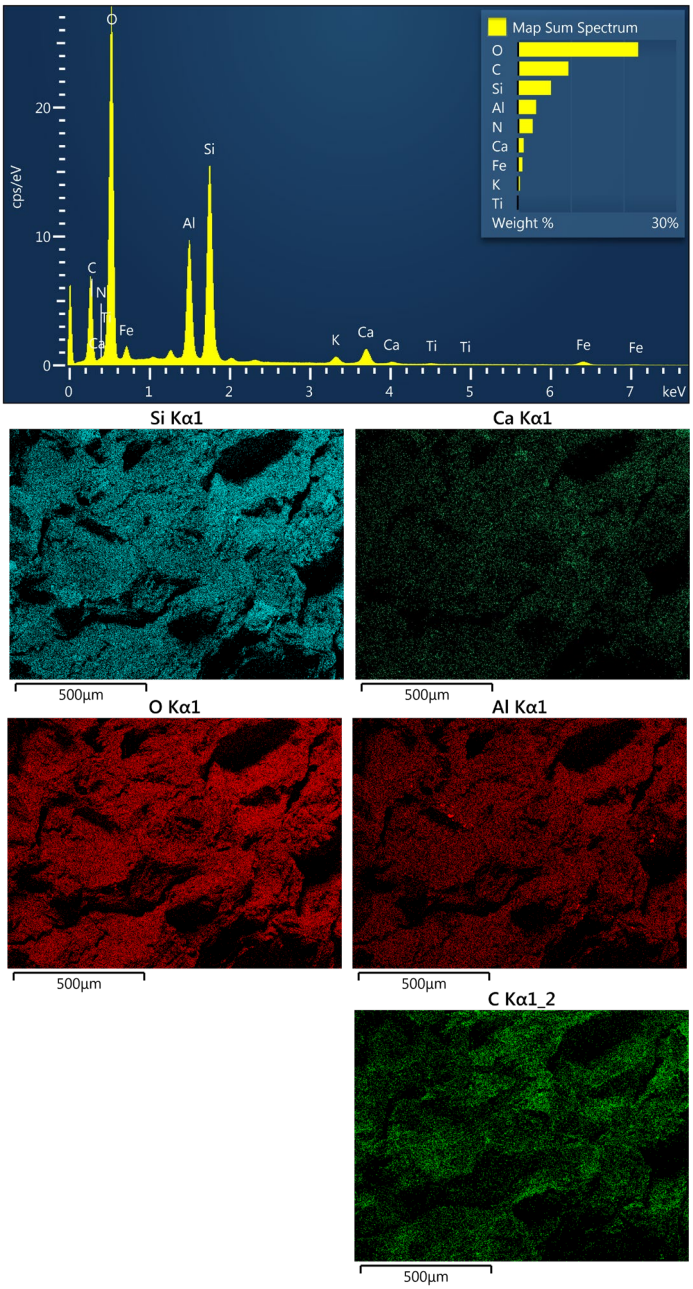

Figure S11: EDS spectrum of sample 21-1 and intensity maps for Si, Ca, O, Al and C. Brighter colour denote higher intensity.

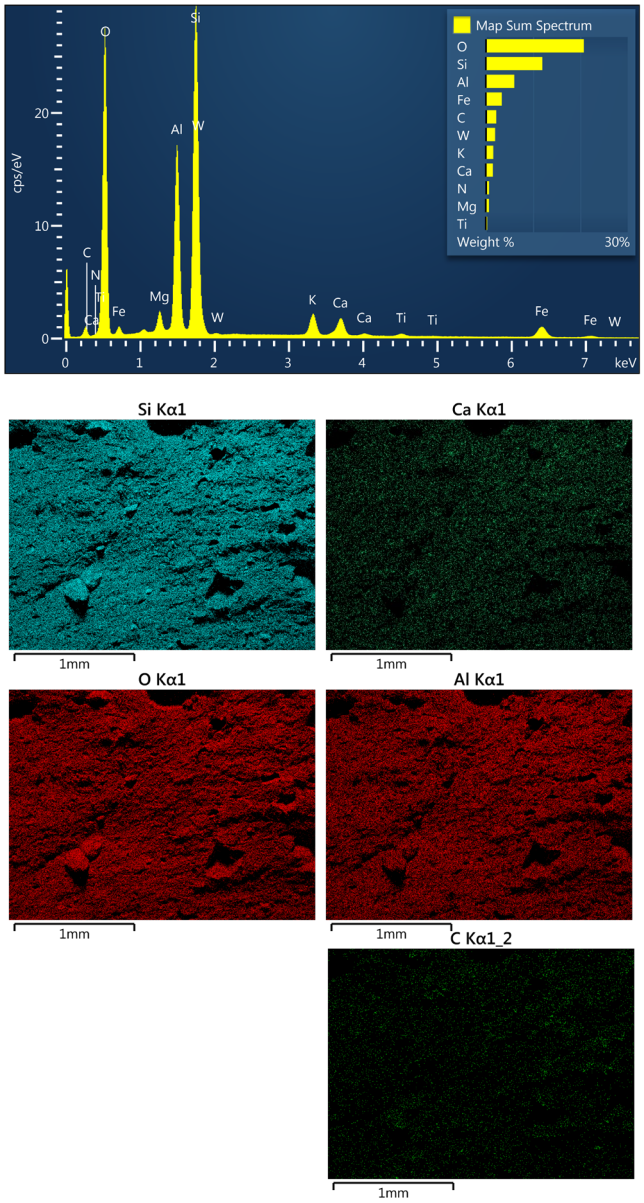

Figure S12: EDS spectrum of sample 15-10 and intensity maps for Si, Ca, O, Al and C. Brighter colour denote higher intensity.